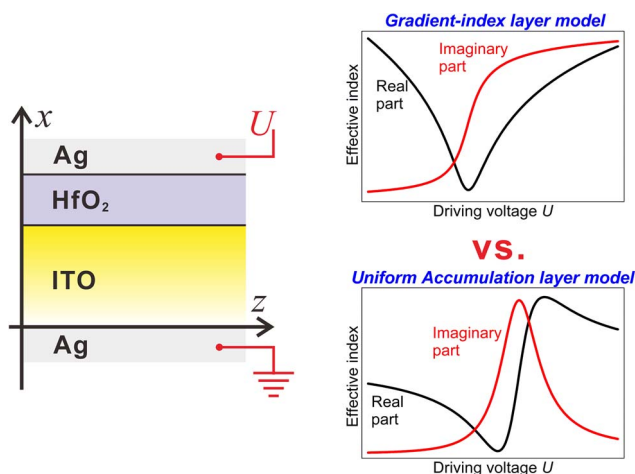


# Discussion of Two Ways of Optically Modeling Indium–Tin–Oxide Layers in Slot Waveguides for Waveguide Analysis

Volume 8, Number 1, February 2016

Min-Suk Kwon



# Discussion of Two Ways of Optically Modeling Indium–Tin–Oxide Layers in Slot Waveguides for Waveguide Analysis

Min-Suk Kwon

School of Electrical and Computer Engineering, Ulsan National Institute of Science and Technology (UNIST), Ulsan 689-798, Korea

DOI: 10.1109/JPHOT.2015.2508421

1943-0655 © 2015 IEEE. Translations and content mining are permitted for academic research only.

Personal use is also permitted, but republication/redistribution requires IEEE permission.

See [http://www.ieee.org/publications\\_standards/publications/rights/index.html](http://www.ieee.org/publications_standards/publications/rights/index.html) for more information.

Manuscript received November 19, 2015; revised December 7, 2015; accepted December 8, 2015. Date of publication December 17, 2015; date of current version December 22, 2015. This work was supported in part by the Basic Science Research Program through the National Research Foundation of Korea funded by the Ministry of Education under Grant 2013R1A1A2A10062227 and in part by the 2015 Research Fund (1.150123) of Ulsan National Institute of Science and Technology. Corresponding author: M.-S. Kwon (e-mail: mskwon@unist.ac.kr).

**Abstract:** Slot waveguides (e.g., metal–insulator–metal (MIM) waveguides) with an indium–tin–oxide (ITO) layer in their slot regions are promising as compact intensity modulators. To analyze such waveguides, a uniform-accumulation layer model is usually used. In this model, the ITO layer is treated as a stack of a layer with untuned permittivity and a layer with permittivity tuned by driving voltage, which is called an accumulation layer. However, rigorous analysis requires a gradient-index layer model in which the ITO layer is treated as a layer with a continuously varying permittivity distribution. It is necessary to check whether the uniform-accumulation layer model results in correct analysis in comparison with the gradient-index layer model. This paper analyzes an ITO-based MIM-type slot waveguide using the two models. Compared with the analysis based on the gradient-index layer model, the analysis based on the uniform-accumulation layer model becomes incorrect if the driving voltage is large, particularly when it is around the value for which the real part of the accumulation layer permittivity is equal to zero. Therefore, this paper shows that the uniform-accumulation layer model should be used just for small driving voltage with the accumulation layer thickness determined appropriately. This paper may correct misunderstanding of the properties of ITO-based slot waveguides.

**Index Terms:** Waveguides, waveguide devices, optical properties of photonic materials.

## 1. Introduction

Indium-tin-oxide (ITO) is representative transparent conducting oxide and it is indispensable for liquid crystal displays and thin-film solar cells. Recently, ITO has been extending its applications into the field of integrated photonics since Feigenbaum *et al.* reported that the refractive index of ITO can be significantly tuned by electrically accumulating free carriers in it [1]. In other words, ITO is considered as an effectively tunable material for dynamically controllable waveguide devices, especially electroabsorption modulators [2]–[12]. A variety of ITO-based electroabsorption modulators have been theoretically investigated [5]–[9], [11], [12], and a few of them have been experimentally studied [3], [4], [10].

In order to tune the refractive index of ITO, an electrostatic field is applied to ITO across an insulator layer by driving voltage, and free carriers are accumulated within a very short distance from the ITO-insulator interface, according to the Thomas–Fermi screening theory [3]. This means that the refractive index of ITO changes only in a very narrow region. Therefore, ITO can effectively control the characteristics of a waveguide mode when a thin ITO layer is located in the slot region of a slot waveguide such as metal-insulator-metal (MIM) waveguides [3], [5], [9], hybrid plasmonic waveguides [4], [7]–[9], and silicon slot waveguides [11]–[13]. For analysis of such slot waveguides, the ITO layer has been mainly modeled as a stack of a homogeneous layer with the initial carrier concentration  $N_0$  of the ITO layer and an accumulation layer with uniform carrier concentration  $N_a$  increased electrostatically [2]–[13]. This is hereafter called a uniform accumulation layer model. As  $N_a$  increases, the real part of the dielectric constant  $\epsilon_{\text{ITO},a}$  of the accumulation layer,  $\text{Re}[\epsilon_{\text{ITO},a}]$  decreases and becomes negative (this can be checked from Fig. 3(b)). Around the value of  $N_a$  for which  $\text{Re}[\epsilon_{\text{ITO},a}] = 0$ , the imaginary part of the effective index  $n_{\text{eff}}$  of a slot waveguide mode,  $\text{Im}[n_{\text{eff}}]$  is maximized, and the real part of  $n_{\text{eff}}$ ,  $\text{Re}[n_{\text{eff}}]$  swings between valley and peak values. These are called the epsilon-near-zero (ENZ) properties of ITO-based slot waveguides [6], [9], [12]–[14]. The ENZ properties seem fascinating since they enable very compact electroabsorption [6], [9], [12] and electrorefraction [13] modulators to be devised.

However, the ENZ properties have been theoretically anticipated from simulations based on the uniform accumulation layer model. Moreover, there is uncertainty in determining the thickness of the accumulation layer,  $t_a$ . Different values of  $t_a$  have been used: 1 nm in [6], [10], [11], [13]; 3 nm in [9]; 5 nm in [1], [12]; and 8 nm in [3]. The uncertainty exists since the carriers induced electrostatically by the driving voltage are actually accumulated in the whole ITO layer although the carrier concentration rapidly decreases as the distance from the ITO-insulator interface increases. The uncertainty even raises a question as to whether the ENZ properties are observable when the ITO layer is rigorously modeled as a layer with a gradient-index distribution. The question leads to checking the validity of the uniform accumulation layer (UAL) model as compared to the gradient-index layer (GIL) model. This paper compares analysis results of an ITO-based MIM-type slot waveguide, which are based on the two models, and shows that the ENZ properties are artifacts coming from the UAL model. In other words, this paper demonstrates that the UAL model is valid only for small driving voltage with the accumulation layer thickness determined appropriately.

## 2. Carrier Concentration and Dielectric Constant Distributions

The investigated ITO-based MIM-type slot waveguide consists of a semi-infinite silver (Ag) layer, an ITO layer of thickness ( $t_{\text{ITO}}$ ) 10 nm [4], [11]–[13], a hafnium oxide ( $\text{HfO}_2$ ) layer of thickness ( $t_{\text{HfO}}$ ) 5 nm [6], [9], [13], and another semi-infinite Ag layer. The layer of  $\text{HfO}_2$ , a well-known high- $\kappa$  dielectric, is the insulator layer required to electrostatically accumulate free carriers in the ITO layer. The waveguide structure is schematically shown in Fig. 1. The layers are perpendicular to the  $x$ -axis, and the fundamental mode of the slot waveguide propagates along the  $z$ -axis. The major electric field component of the slot waveguide mode is parallel to the  $x$ -axis and strongly confined in the slot region (i.e., the ITO and  $\text{HfO}_2$  layers) along the  $x$ -axis due to the nature of a surface plasmon polariton or the discontinuity of a surface-normal electric field component. Since the confinement along the  $x$ -axis dominates the characteristics of the slot waveguide mode, the slot waveguide is assumed to be uniform in the  $y$ -axis. Then, the slot waveguide mode is purely transverse-magnetic (TM). Driving voltage  $U$  is applied between the Ag layers to accumulate free carriers in the ITO layer. The refractive indices of Ag and  $\text{HfO}_2$ ,  $n_{\text{Ag}}$  and  $n_{\text{HfO}}$  are  $0.5029 + i10.95$  and  $1.980$  [6] at the telecom wavelength of  $1.55 \mu\text{m}$ .  $n_{\text{Ag}}$  is calculated from the Drude–Lorentz model of Ag [15]. The wavelength  $\lambda$  is  $1.55 \mu\text{m}$  in the following calculations, but calculations at other wavelengths give results similar to the following.

The analysis of the slot waveguide starts from determining the carrier concentration distribution  $N(x)$  of the ITO layer for a given value of  $U$ . This step follows what is explained in [3].

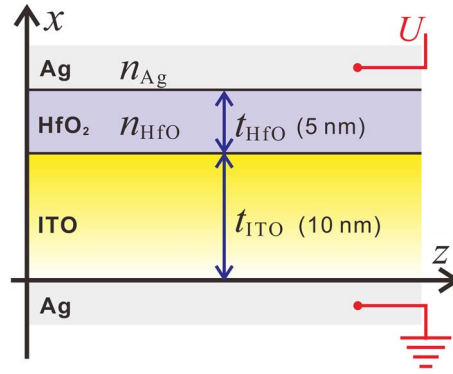


Fig. 1. Schematic diagram of the ITO-based metal–insulator–metal-type slot waveguide investigated in this paper. The structure is uniform in the  $y$  axis, and the  $z$  axis is the propagation direction of this waveguide. The driving voltage  $U$  is applied between the two Ag layers.

According to the Thomas–Fermi screening theory,  $N(x)$  is given by

$$N(x) = N_0[1 + e\phi(x)/E_F]^{3/2} \quad (1)$$

where  $e$  is the elementary charge and  $\phi(x)$  is the electric potential associated with  $N(x)$ . The Fermi energy  $E_F$  is expressed by

$$E_F = \hbar^2(3\pi^2 N_0)^{2/3}/(8\pi^2 m_{\text{eff}}) \quad (2)$$

where  $\hbar$  is the Planck constant, and  $m_{\text{eff}}$  is the effective electron mass in ITO.  $\phi(x)$  is determined by solving the second-order nonlinear differential equation derived from Poisson's equation and (1), which is

$$\frac{d^2\phi(x)}{dx^2} = \frac{eN_0\{[1 + e\phi(x)/E_F]^{3/2} - 1\}}{\epsilon_0\epsilon_{\text{ITO,S}}} \quad (3)$$

subject to the boundary conditions that

$$d\phi/dx|_{x=t_{\text{ITO}}} = (U/t_{\text{HfO}_2})(\epsilon_{\text{HfO}_2,\text{S}}/\epsilon_{\text{ITO,S}}) \text{ and } \phi(-\infty) = 0. \quad (4)$$

$\epsilon_{\text{ITO,S}}$  and  $\epsilon_{\text{HfO}_2,\text{S}}$  are the static dielectric constants of ITO and  $\text{HfO}_2$ , respectively, which are 9.3 and 25;  $\epsilon_0$  is the vacuum permittivity. When  $m_e$  is the free electron mass,  $m_{\text{eff}} = 0.35m_e$ . The carrier concentration  $N_a$  of the accumulation layer is given by  $N_0 + \int_0^{t_{\text{ITO}}} [N(x) - N_0] dx/t_a$ . The differential equation in (3) is solved by using the `bvp4c` function of MATLAB. The calculated distributions of  $N(x)$  for various values of  $U$  are shown in Fig. 2(a).  $N_0$  is chosen to be  $1 \times 10^{19} \text{ cm}^{-3}$ .  $N$  decreases rapidly from the ITO– $\text{HfO}_2$  interface, and its peak value increases with  $U$ . The inset of Fig. 2(a) shows that  $N$  becomes equal to a particular value  $N_{\text{ENZ}} = 6.49 \times 10^{20} \text{ cm}^{-3}$  at  $x = 9.86, 9.59,$  and  $9.42 \text{ nm}$  for  $U = 2, 3,$  and  $4 \text{ V}$ , respectively (what  $N_{\text{ENZ}}$  means becomes clear after (5)). The relations of  $N_a$  to  $U$  for various values of  $t_a$  are shown in Fig. 2(b). The value of  $U$  which makes  $N_a$  equal to  $N_{\text{ENZ}}$  increases with  $t_a$ . This means that in the case of the uniform accumulation layer model, the ENZ properties are obtained from different values of  $U$  depending on chosen values of  $t_a$ . Those values of  $U$  are 1.16, 2.31, and 3.46 V for  $t_a = 0.5, 1.0,$  and  $1.5 \text{ nm}$ , respectively.

Based on the Drude model, the dielectric constant  $\epsilon_{\text{ITO}}(x)$  of the ITO layer is determined from  $N(x)$ , which is given by

$$\epsilon_{\text{ITO}}(x) = \epsilon_\infty - e^2 N(x)/[(\epsilon_0 m_{\text{eff}})(\omega^2 + i\gamma\omega)] \quad (5)$$

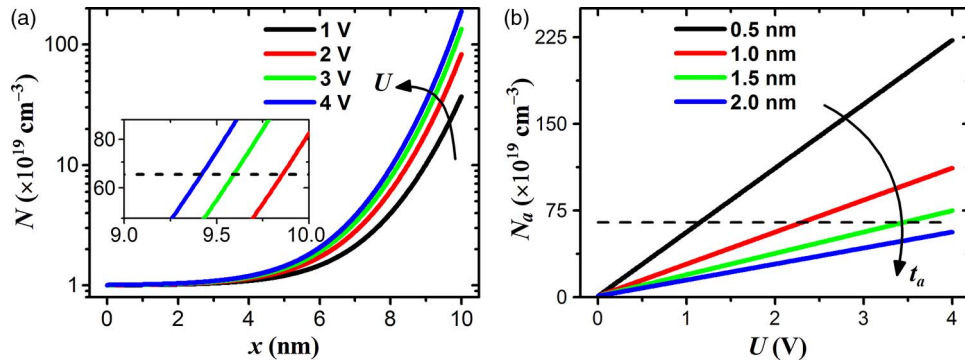


Fig. 2. (a) Distributions of  $N(x)$  for  $U = 1, 2, 3,$  and  $4$  V. The inset clearly shows that  $N$  is equal to  $N_{\text{ENZ}} = 6.49 \times 10^{20} \text{ cm}^{-3}$  at a smaller value of  $x$  for a larger value of  $U$ . (b) Relations of  $N_a$  to  $U$  for  $t_a = 0.5, 1.0, 1.5,$  and  $2.0$  nm. The dashed line corresponds to  $N_a = N_{\text{ENZ}}$ .

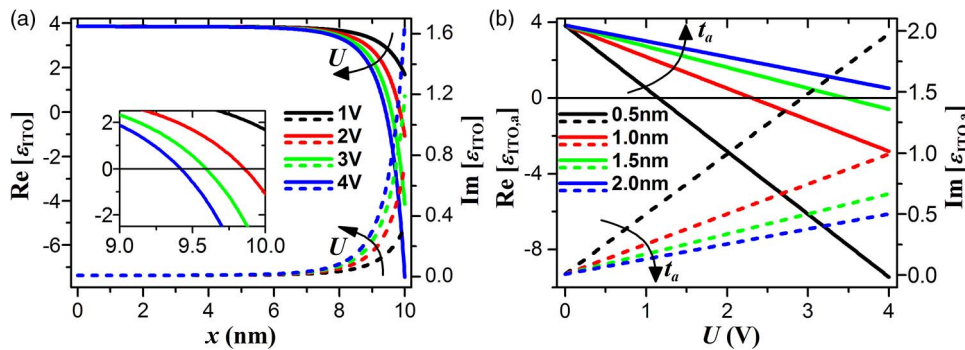


Fig. 3. (a) Distributions of the real and imaginary parts of  $\epsilon_{\text{ITO}}(x)$   $\text{Re}[\epsilon_{\text{ITO}}]$  and  $\text{Im}[\epsilon_{\text{ITO}}]$  for  $U = 1, 2, 3,$  and  $4$  V. (Inset)  $\text{Re}[\epsilon_{\text{ITO}}] = 0$  at the same values of  $x$  as those found in the inset of Fig. 2(a). (b) Relations of the real and imaginary parts of  $\epsilon_{\text{ITO},a}$   $\text{Re}[\epsilon_{\text{ITO},a}]$  and  $\text{Im}[\epsilon_{\text{ITO},a}]$  to  $U$  for  $t_a = 0.5, 1.0, 1.5,$  and  $2.0$  nm. The thin solid line corresponds to  $\text{Re}[\epsilon_{\text{ITO},a}] = 0$ . In (a) and (b), the solid lines represent the real parts, and the dashed lines represent the imaginary parts.

where  $\epsilon_\infty$  is the high frequency dielectric constant,  $\gamma$  is the collision frequency, and  $\omega$  is the angular frequency.  $\epsilon_\infty$  is 3.9, and  $\gamma$  is  $1.8 \times 10^{14} \text{ s}^{-1}$ . The dielectric constant  $\epsilon_{\text{ITO},0}$  of the untuned ITO layer and  $\epsilon_{\text{ITO},a}$  are calculated from (5) by substituting  $N_0$  and  $N_a$  for  $N(x)$ , respectively. The distributions of the real and imaginary parts of  $\epsilon_{\text{ITO}}(x)$ ,  $\text{Re}[\epsilon_{\text{ITO}}]$  and  $\text{Im}[\epsilon_{\text{ITO}}]$ , for the values of  $U$  are shown in Fig. 3(a). As checked from (5),  $\text{Re}[\epsilon_{\text{ITO}}] = 0$  if  $N$  is equal to  $\epsilon_0 \epsilon_\infty m_{\text{eff}}(\omega^2 + \gamma^2)/e^2$ , which has been denoted by  $N_{\text{ENZ}}$ . Therefore, the inset of Fig. 3(a) shows that  $\text{Re}[\epsilon_{\text{ITO}}] = 0$  at  $x = 9.86, 9.59,$  and  $9.42$  nm for  $U = 2, 3,$  and  $4$  V, respectively. The relations of  $\text{Re}[\epsilon_{\text{ITO},a}]$  and  $\text{Im}[\epsilon_{\text{ITO},a}]$ , which is the imaginary part of  $\epsilon_{\text{ITO},a}$ , to  $U$  for the values of  $t_a$  are shown in Fig. 3(b). As deduced from Fig. 2(b),  $\text{Re}[\epsilon_{\text{ITO},a}] = 0$  at  $U = 1.16, 2.31,$  and  $3.46$  V for  $t_a = 0.5, 1.0,$  and  $1.5$  nm, respectively.

### 3. Comparison of the Analysis Results Based on the Gradient-Index Layer Model and the Uniform Accumulation Layer Model

To analyze the slot waveguide based on the gradient-index layer (GIL) model of the ITO layer, the ITO layer is treated as a stack of  $M$  layers with the same thickness  $\Delta t = t_{\text{ITO}}/M$ . The refractive index distribution  $n_{\text{ITO}}(x)$  is given by  $[\epsilon_{\text{ITO}}(x)]^{1/2}$ , and the refractive index of the  $j$ -th layer is given by  $n_{\text{ITO}}(j\Delta t)$  for  $j = 1 \cdots M$ . Then, the slot waveguide is a planar waveguide consisting of  $M + 1$  layers bounded by Ag, the  $(M + 1)$ -th layer of which is the  $\text{HfO}_2$  layer. In the case of the

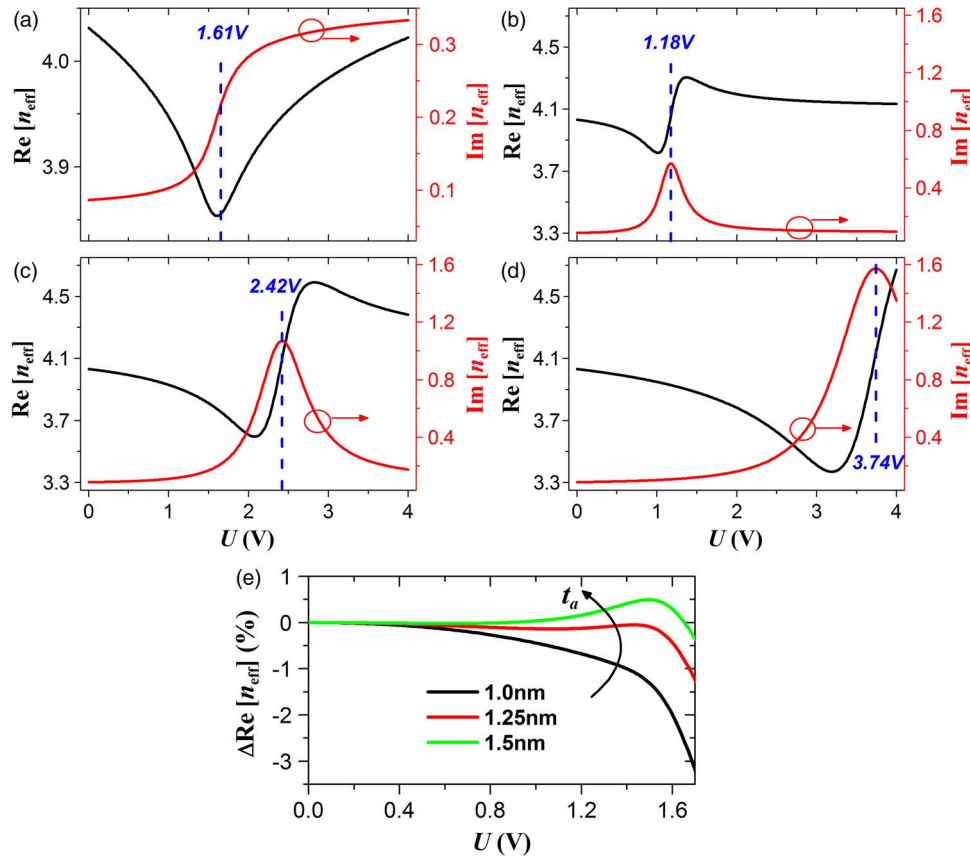


Fig. 4. Effective index  $n_{\text{eff}}$  of the slot waveguide versus  $U$ . (a) Relations of  $\text{Re}[n_{\text{eff}}]$  and  $\text{Im}[n_{\text{eff}}]$  to  $U$  which are obtained from the analysis based on the GIL model. (b)–(d) Such relations which are obtained from the analysis based on the UAL model for  $t_a = 0.5, 1.0,$  and  $1.5$  nm, respectively. (e) Relation of the fractional error in  $\text{Re}[n_{\text{eff}}]$  related to the UAL model  $\Delta\text{Re}[n_{\text{eff}}]$  to  $U$ .

analysis based on the uniform accumulation layer (UAL) model, the slot waveguide is a planar waveguide consisting of the unbiased ITO layer of refractive index  $n_{\text{ITO},0} (= (\epsilon_{\text{ITO},0})^{1/2})$  and thickness  $(\hat{t}_{\text{ITO}} - t_a)$ , the accumulation layer of refractive index  $n_{\text{ITO},a} (= (\epsilon_{\text{ITO},a})^{1/2})$  and thickness  $t_a$ , and the  $\text{HfO}_2$  layer, all of which are bounded by Ag. The planar waveguides are analyzed by using the well-known transfer matrix method [16], [17]. The eigenvalue equation for the effective index  $n_{\text{eff}}$  of the slot waveguide mode is derived from the transfer matrix method and it is solved by using the `fsolve` function of MATLAB. In the case of the analysis based on the GIL model,  $M$  should be determined such that  $n_{\text{eff}}$  converges. The convergence is achieved for  $M \geq 1000$ . Hence,  $M$  is 1000 in the following calculations.

The calculated relations of  $\text{Re}[n_{\text{eff}}]$  and  $\text{Im}[n_{\text{eff}}]$  to  $U$  are shown in Fig. 4. Those in Fig. 4(a) are associated with the GIL model. The relations in Fig. 4(b)–(d) are related to the UAL model with  $t_a = 0.5, 1.0,$  and  $1.5$  nm, respectively. They are definitely different from those in Fig. 4(a). The ENZ properties mentioned above are not observed in Fig. 4(a) but observed in the remaining figures. In the case of the analysis based on the GIL model,  $\text{Im}[n_{\text{eff}}]$  increases with  $U$  and becomes saturated after  $U$  is larger than the value  $U_0 = 1.62$  V for which  $\text{Re}[\epsilon_{\text{ITO}}(x = \hat{t}_{\text{ITO}})] = 0$  (the reason for this change can be found in Fig. 5(a) and (b)). When  $U$  increases from 0 V to 4 V,  $\text{Im}[n_{\text{eff}}]$  increases by 0.247.  $\text{Re}[n_{\text{eff}}]$  slightly decreases and then increases. Its maximum change is 0.178, and its minimum is at  $U = 1.61$  V, which is close to  $U_0$ . In the case of the analysis based on the UAL model, as  $t_a$  increases, the maximum of  $\text{Im}[n_{\text{eff}}]$  increases, and the difference between the maximum and the minimum of  $\text{Re}[n_{\text{eff}}]$  also increases (the reason for



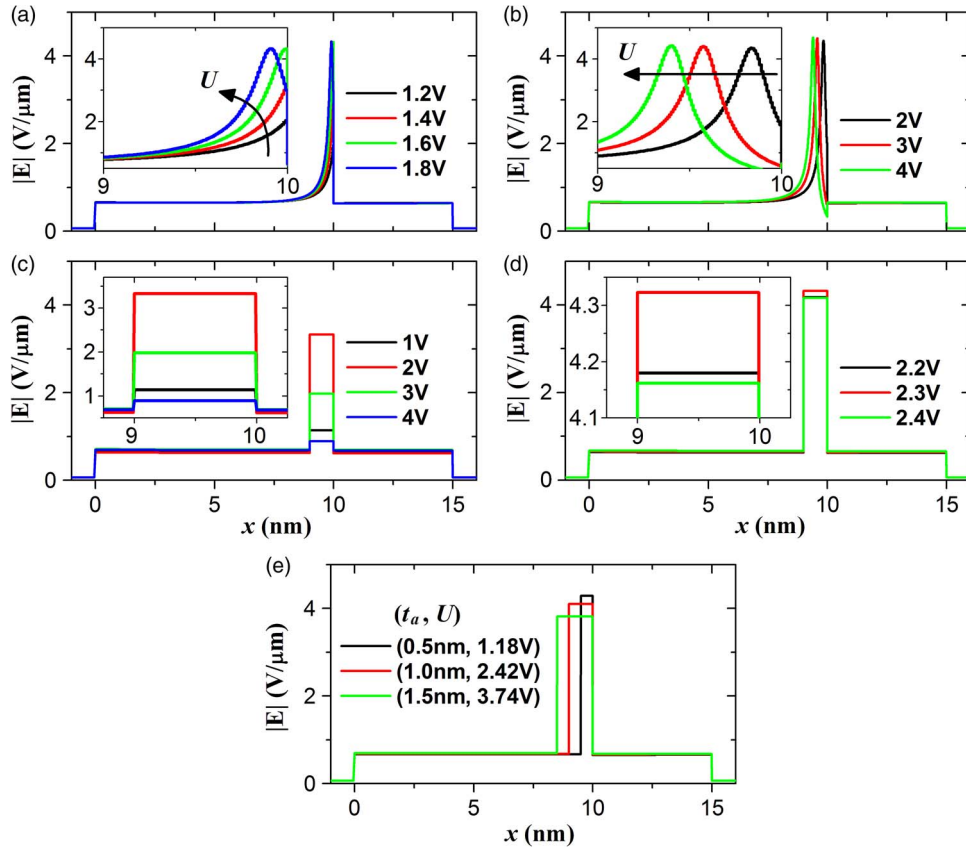


Fig. 5. Distributions of the electric field  $E$  of the slot waveguide mode. The distributions of  $|E(x)|$  in (a) and (b) are obtained from the analysis based on the GIL model. Those in (c)–(e) are obtained from the analysis based on the UAL model. The insets show the enlarged distributions near the ITO-HfO<sub>2</sub> interface. (e) Distributions for  $(t_a, U) = (0.5 \text{ nm}, 1.18 \text{ V})$ ,  $(1.0 \text{ nm}, 2.42 \text{ V})$ , and  $(1.5 \text{ nm}, 3.74 \text{ V})$ .

such changes is explained in conjunction with Fig. 5(c) and (d)). The maxima of  $\text{Im}[n_{\text{eff}}]$  are at  $U = 1.18, 2.42,$  and  $3.74 \text{ V}$  for  $t_a = 0.5, 1.0,$  and  $1.5 \text{ nm}$ , respectively. The values of  $U$  are slightly larger than those at which  $\text{Re}[\epsilon_{\text{ITO},a}] = 0$ . The results in Fig. 4(b)–(d) indicate that an electroabsorption or electrorefraction modulator based on the slot waveguide has different characteristics calculated, such as driving voltage, extinction ratio, and phase change, depending on a chosen value of  $t_a$ . The comparison of the results in Fig. 4 demonstrates that the ENZ properties do not exist when the slot waveguide is rigorously analyzed using the GIL model and they are just illusory characteristics resulting from the UAL model. Therefore, the UAL model gives misinformation about the largest extinction ratio of an electroabsorption modulator based on the slot waveguide and the driving voltage for that extinction ratio. Moreover, an electrorefraction modulator based on the slot waveguide does not work properly since there is no pair of driving voltages for which  $\text{Im}[n_{\text{eff}}]$  does not change but  $\text{Re}[n_{\text{eff}}]$  changes quite much. Although the UAL model does not yield correct analysis of the slot waveguide, especially when  $U$  approaches the value for which  $\text{Re}[\epsilon_{\text{ITO},a}]$  is equal to zero, it makes the analysis very simple. As shown in Fig. 4(e), if  $t_a = 1.25 \text{ nm}$ , the fractional error in  $\text{Re}[n_{\text{eff}}]$  related to the UAL model,  $\Delta\text{Re}[n_{\text{eff}}]$  is almost close to 0% for  $U < U_0$ . This result means that the UAL model with the appropriately determined value of  $t_a$  can be still used to analyze the slot waveguide only when  $U < U_0$ .

It is necessary to find why the two models of the ITO layer result in the different relations of  $n_{\text{eff}}$  to  $U$ . The reason for that can be elucidated by the distribution of the electric field  $\mathbf{E}(x)$  of the

slot waveguide mode. The distributions of  $|\mathbf{E}(x)|$  for various values of  $U$ , which are calculated using the GIL model, are shown in Fig. 5(a) and (b). When  $U < U_0$ , the maximum of  $|\mathbf{E}(x)|$  is at  $x = t_{\text{ITO}}$ . As  $U$  increases further, the spike that  $\mathbf{E}$  is highly enhanced shifts to  $x = 0$ , but its height does not change significantly. The positions of the spike are at  $x = 9.84, 9.58,$  and  $9.40$  nm for  $U = 2, 3,$  and  $4$  V, respectively. They are almost coincident with those at which  $\text{Re}[\varepsilon_{\text{ITO}}] = 0$ . From the boundary condition for a surface-normal electric field component,  $|\mathbf{E}((j+1)\Delta t)| \approx |\varepsilon_{\text{ITO}}(j\Delta t)| |\mathbf{E}(j\Delta t)| / |\varepsilon_{\text{ITO}}((j+1)\Delta t)|$ , and hence  $|\mathbf{E}|$  increases when  $|\varepsilon_{\text{ITO}}|$  decreases. Since  $|\varepsilon_{\text{ITO}}|$  is minimized near the position at which  $\text{Re}[\varepsilon_{\text{ITO}}] = 0$ ,  $|\mathbf{E}|$  is maximized there, and the spike exists. As  $U$  becomes larger than  $U_0$ , the position at which  $\text{Re}[\varepsilon_{\text{ITO}}] = 0$  shifts to  $x = 0$  as shown in Fig. 3(a), and the spike also shifts to  $x = 0$ . In addition, the metal-like region of the ITO layer widens from the ITO-HfO<sub>2</sub> interface, and hence  $\text{Im}[n_{\text{eff}}]$  slightly increases. The distributions of  $|\mathbf{E}(x)|$  related to the UAL model with  $t_a = 1.0$  nm are shown for various values of  $U$  in Fig. 5(c) and (d). As  $U$  approaches the value for which  $\text{Re}[\varepsilon_{\text{ITO,a}}] = 0$ ,  $\mathbf{E}$  is more strongly confined in the accumulation layer due to the same boundary condition as above. Otherwise, the confinement of  $\mathbf{E}$  in the accumulation layer is not strong. Therefore,  $\text{Im}[n_{\text{eff}}]$  is maximized when  $\text{Re}[\varepsilon_{\text{ITO,a}}] = 0$ . Although the strong enhancement of  $\mathbf{E}$  persists for  $U > U_0$  in the case of the GIL model, in the case of the UAL model, it exists only when  $U$  is around the value for which  $\text{Re}[\varepsilon_{\text{ITO,a}}] = 0$ . This difference results in the different relations of  $n_{\text{eff}}$  to  $U$  in Fig. 4. As shown in Fig. 5(e), the larger  $t_a$  is, the larger fraction of the slot waveguide mode is confined in the accumulation layer for the larger value of  $U$  for which  $\text{Re}[\varepsilon_{\text{ITO,a}}]$  is almost equal to zero. Therefore, the absorption of the mode by the accumulation layer increases with  $t_a$ , as does the maximum of  $\text{Im}[n_{\text{eff}}]$ , as shown in Fig. 4.

#### 4. Conclusion

In summary, the MIM-type ITO-based slot waveguide has been analyzed using the UAL model and the GIL model. The UAL model makes the analysis simple, but it should be checked whether the UAL model results in correct analysis. To do so, the analysis based on the UAL model has been compared to the analysis based on the GIL model which enables correct analysis. The comparison of the analysis results based on the two models has indicated that the UAL model is valid only when  $t_a$  is appropriately chosen and  $U$  is smaller than the value for which  $\text{Re}[\varepsilon_{\text{ITO}}] = 0$  at the ITO-HfO<sub>2</sub> interface. The ENZ properties are not observed in the analysis result based on the GIL model. The same conclusion can be deduced from other ITO-based slot waveguides such as hybrid plasmonic waveguides and silicon slot waveguides. Therefore, the GIL model has to be used to rigorously analyze ITO-based slot waveguides with large driving voltage applied to them.

#### References

- [1] E. Feigenbaum, K. Diest, and H. A. Atwater, "Unity-order index change in transparent conducting oxides at visible frequencies," *Nano Lett.*, vol. 10, no. 10, pp. 2111–2116, Oct. 2010.
- [2] V. Babicheva, A. Boltasseva, and A. V. Lavrinenko, "Transparent conducting oxides for electro-optical plasmonic modulators," *Nanophoton.*, vol. 4, no. 1, pp. 165–185, Jan. 2015.
- [3] A. Melikyan *et al.*, "Surface plasmon polariton absorption modulator," *Opt. Exp.*, vol. 19, no. 9, pp. 8855–8869, Apr. 2011.
- [4] V. J. Sorger, N. D. Lanzillotti-Kimura, R.-M. Ma, and X. Zhang, "Ultra-compact silicon nanophotonic modulator with broadband response," *Nanophoton.*, vol. 1, no. 1, pp. 17–22, Jul. 2012.
- [5] A. V. Krasavin and A. V. Zayats, "Photonic signal processing on electronic scales: Electro-optical field-effect nanoplasmonic modulator," *Phys. Rev. Lett.*, vol. 109, no. 5, Aug. 2012, Art. ID 053901.
- [6] A. P. Vasudev, J.-H. Kang, X. Liu, and M. Brongersma, "Electro-optical modulation of a silicon waveguide with an 'epsilon-near-zero' material," *Opt. Exp.*, vol. 21, no. 22, pp. 26387–26397, Nov. 2013.
- [7] C. Huang, R. J. Lamond, S. K. Pickus, Z. R. Li, and V. J. Sorger, "A sub- $\lambda$ -size modulator beyond the efficiency-loss limit," *IEEE Photon. J.* vol. 5, no. 4, Aug. 2013, Art. ID 2202411.
- [8] C. Ye, S. Khan, Z. R. Li, E. Simsek, and V. J. Sorger, " $\lambda$ -size ITO and graphene-based electro-optic modulators on SOI," *IEEE J. Sel. Topics Quantum Electron.*, vol. 20, no. 4, Jul./Aug. 2014, Art. ID 3400310.
- [9] S. Zhu, G. Q. Lo, and D. L. Kwong, "Design of an ultra-compact electro-absorption modulator comprised of a deposited TiN/HfO<sub>2</sub>/ITO/Cu stack for CMOS backend integration," *Opt. Exp.*, vol. 22, no. 15, pp. 17930–17947, Jul. 2014.



- [10] H. W. Lee *et al.*, "Nanscale conducting oxide plasmistor," *Nano Lett.*, vol. 14, no. 11, pp. 6463–6468, Nov. 2014.
- [11] J. T. Kim, "Silicon optical modulators based on tunable plasmonic directional couplers," *IEEE J. Sel. Topics Quantum Electron.*, vol. 21, no. 4, Jul./Aug. 2015, Art. ID 3300108.
- [12] H. Zhao, Y. Wang, A. Capretti, L. D. Negro, and J. Klamkin, "Broadband electroabsorption modulators design based on epsilon-near-zero indium tin oxide," *IEEE J. Sel. Topics Quantum Electron.*, vol. 21, no. 4, Jul./Aug. 2015, Art. ID 3300207.
- [13] J. Baek, J.-B. You, and K. Yu, "Free-carrier electro-refraction modulation based on a silicon slot waveguide with ITO," *Opt. Exp.*, vol. 23, no. 12, pp. 15 863–14 876, Jun. 2015.
- [14] Z. Lu, W. Zhao, and K. Shi, "Ultracompact electroabsorption modulators based on tunable epsilon-near-zero-slot waveguides," *IEEE Photon. J.*, vol. 4, no. 3, pp. 735–740, Jun. 2012.
- [15] S. G. Rodrigo, F. J. García-Vidal, and L. Martín-Moreno, "Influence of material properties on extraordinary optical transmission through hole arrays," *Phy. Rev. B, Condens. Matter Mater Phys.*, vol. 77, no. 7, Feb. 2008, Art. ID 075401.
- [16] M.-S. Kwon and S.-Y. Shin, "Simple and fast numerical analysis of multilayer waveguide modes," *Opt. Commun.*, vol. 233, no. 1–3, pp. 119–126, Mar. 2004.
- [17] M.-S. Kwon, "A numerically stable analysis method for complex multilayer waveguides based on modified transfer-matrix equations," *J. Lightw. Technol.*, vol. 27, no. 20, pp. 4407–4414, Oct. 2009.